TOTAL VARIATION WAVELET INPAINTING *

TONY F. CHAN †, JIANHONG SHEN ‡, AND HAO-MIN ZHOU §

Abstract. We consider the problem of filling in missing or damaged wavelet coefficients due to lossy image transmission or communication. The task is closely related to classical inpainting problems, but also remarkably differs in that the inpainting regions are in the wavelet domain. New challenges include that the resulting inpainting regions in the pixel domain are usually not geometrically well defined, as well as that degradation is often spatially inhomogeneous. We propose two related variational models to meet such challenges, which combine the total variation (TV) minimization technique with wavelet representations. The associated Euler-Lagrange equations lead to nonlinear partial differential equations (PDE's) in the wavelet domain, and proper numerical algorithms and schemes are designed to handle their computation. The proposed models can have effective and automatic control over geometric features of the inpainted images including sharp edges, even in the presence of substantial loss of wavelet coefficients, including in the low frequencies. Existence and uniqueness of the optimal inpaintings are also carefully investigated.

1. Introduction. Image inpainting refers to filling in missing or damaged regions (like cracks or scars) in images. In fine art museums, inpainting of degraded paintings is traditionally carried out by professional artists and usually very time consuming, not to mention the risk of completely destroying a precious and world-unique ancient painting due to direct retouching.

Mathematically speaking, inpainting is essentially an interpolation problem, and thus directly overlaps with many other important tasks in computer vision and image processing, including image replacement [41], disocclusion [49, 53], zooming and superresolution [15, 45, 47], and error concealment [42] [64]. The current work has been more motivated and inspired by the error concealment application, which is to automatically recover lost packets information during transmission processes.

The notion of *digital image inpainting* was invented by Bertalmio-Sapiro-Caselles-Balleste in [4], where the authors pioneered a novel inpainting technique based on a 3rd order nonlinear PDE. This work has stimulated the recent wave of interest in geometric image interpolation and inpainting problems, for example, variational PDE models [13], [15], [16], [34], Navier-Stokes equation and fluid dynamic system related methods [3], landmark based inpainting [43], texture inpainting [5], inpainting by vector fields and gray levels [2], inpainting by corresponding maps [27], and morphological component analysis for cartoon and texture inpainting [33]. Very recently, PDE techniques in image inpainting were featured in the article "Filling in Blanks" by Ivars Peterson in the **Science News** (Vol. 161/19, 05/11/2002) [56].

In this paper, we study a generalized (as compared with conventional inpainting) inpainting problem for which data loss occurs in the wavelets domain. The primary motivation for us to study wavelet based image inpainting is that many images are formatted and stored in terms of wavelet coefficients, especially after the release of the new image compression standard JPEG2000, which is largely based on wavelet transforms, including the famous Daubechies 7-9 biorthogonal wavelet decomposition.

*Research supported in part by grants ONR-N00014-03-1-0888, NSF DMS-9973341, DMS-0202565 and DMS-0410062, and NIH contract P 20 MH65166.

† Department of Mathematics, the University of California, Los Angeles, CA90095-1555. email:chan@math.ucla.edu.

‡ Department of Mathematics, the University of Minnesota, 206 Church St. SE Minneapolis, MN 55455. email:jhshen@math.umn.edu.

§ School of Mathematics, Georgia Institute of Technology, Atlanta, GA 30332. email:hmzhou@math.gatech.edu.

Minor damages to compact discs coding JPEG2000 image files and data loss during wireless transmission processes, for example, could both result in the need for filling-in the missing information in the wavelet domain instead of the pixel domain.

Working in the wavelet domain, instead of the pixel domain, changes the nature of the inpainting problem, since damages to wavelet coefficients can create correlated damage patterns in the pixel domain. For instance, for wavelets based image inpainting problems, there usually exists no corresponding regular geometric inpainting regions, which are however necessary for many PDE-based inpainting models in pixel domains. Such lack of spatial geometric regularity of inpainting regions also prohibits many other existent inpainting techniques applied to pixel domains [49]. On the other hand, direct interpolation in the wavelet domain is also problematic. Unlike thresholding-based image denoising [30, 11], wavelets *decoupling* achieved by Besov image models is convenient for componentwise image denoising but *intrinsically insufficient* for direct interpolation in the wavelets domain. Section 3.1 will further clarify this key point.

For this reason, many contemporary error concealment methods for JPEG (built upon discrete cosine transforms (DCT)) or JPEG2000 (upon wavelets) images require the additional control of regularity in pixel domains, in addition to direct operations in transformed domains (i.e., DCT or wavelets). Such examples include Hemami-Gray's bi-cubic Coons surface [40], non-uniform rational B-spline (NURBS) by Park-Lee [55] and by Cheng et. al. [23], Niu-Poston's harmonic postprocessing techniques [54], Sapiro and collaborators' separate reconstruction techniques for structures and textures [58], and least square minimization in wavelet-domain reconstructions [57]. However, these JPEG based error concealment methods usually work on images that have already been partitioned into 8×8 or 16×16 blocks. Each missing or damaged block corresponds to a well defined square region to be filled-in in the pixel domain. Our present work however makes no *a priori* assumption on block partitioning.

An important guiding principle for our new models is that even though the primary goal is to fill in the missing coefficients in the wavelet domain, it is important to control the regularity in the pixel domain, so that the inpainted images retain important geometrical features such as sharp edges, especially when noise is present.

Such considerations have motivated the variational PDE approach in our current work. The variational PDE technique has been widely used in numerous applications such as image segmentation [10] [18] [65], restoration [19], [59], compression [21] [31], zooming [48], and conventional image inpainting [3] [4] [13] [16] [34].

The growing impact of variational PDE techniques in image processing is mainly due to their capability and flexibility in controlling geometrical features of images. For example, total variation (TV) minimization, which leads to a curvature term in the corresponding Euler-Lagrange equation, can retain sharp edges in image restoration. In this paper, we select TV minimization to facilitate the inpainting process so that the missing or damaged coefficients can be filled in to faithfully restore geometric image features. In addition, the TV minimization can also systematically suppress the noise in the images. All the above properties make TV minimization a crucial ingredient for wavelets based image inpainting. As detailed later in Section 3.1, the TV Radon measure, with its rich geometric properties, cannot be replaced by any Besov norm, or equivalently, be controlled sheerly by the sizes of wavelets coefficients.

It is worth pointing out that the idea of using TV minimization together with wavelet representations in image processing has been proposed by different research groups. For example, in an earlier work of the first and third authors [22], models of

combining wavelets and TV minimization have been studied for image denoising and compression. Later, Durand-Froment [32] use TV minimization in conjunction with wavelets to eliminate pseudo oscillations in image restoration. Candes-Guo [7] use TV minimization to clean up oscillations from curvelet reconstructions, and Starck-Elad-Donoho [62] decomposes images using combination of TV norm and l_1 wavelet coefficient norm. Interesting work on combining TV with wavelets for general image restoration problems has also been studied by Malgouyres [46]. More recently, another interesting and related study has been conducted by Candes-Romberg-Tao [8], in which a probabilistic theory has been developed for the conditions of exact reconstruction of small support functions, such as impulses, from their incomplete frequency information by minimizing convex functionals including l_0, l_1 and TV norms. In [9], Candes-Tao has further analyzed the reconstruction error in probability sense by minimizing l_1 norm for the functions whose frequency coefficients obey a power-law decay property.

We now describe briefly our main approach to the wavelet inpainting problem and some of the main results in our paper. We propose two related TV-wavelet inpainting models, one for noise-free channels while the other for noisy ones. Mathematically, the noise-free model is non-parametric, while the other is inevitably parametric in order to incorporate the noise information (e.g., noise variances). We then explain the major difference between TV-wavelets inpainting and the well-known thresholding methods for wavelet-based image denoising [11, 29, 30]. Wavelets inpainting requires *coupled* wavelets regularities such as TV to correlate the missing and existent components, whereas in classical denoising, *decoupling* plays a fundamental role in simple and componentwise algorithms. For the theoretical part of the paper, we rigorously prove the existence of solutions to our wavelet inpainting models. The proof is non-standard because boundedness of the solution does not follow from standard arguments due to the lack of data in the inpainting regions and needs to be first established. We also showed a counter-example to show that in general uniqueness cannot be established for our models. We also explain why the non-uniqueness for such generalized inpainting problems (i.e., loss of linearly transformed data) is not so straightforward as the classical inpainting problems (e.g., Chan and Shen [15]). For practical applications in the error concealment of wavelets-based image communication, we develop the necessary (though by no means optimal) numerical algorithms and demonstrate surprisingly good experimental performance of the models for both generic natural images and synthetic ones with salient geometric ingredients. The two key features are (a) unlike controlled optimal wavelets analysis or compression, the data loss is random and spread across all resolutions levels; and (b) unlike lossy wavelets synthesis or decompression algorithms [25, 63], TV-wavelets hybrid inpainting successfully suppress the notorious Gibbs' phenomenon due to the TV control. Our experiments show that even with substantial loss of wavelet coefficients (up to 50%, including low frequencies), our models are able to reconstruct the original image remarkably well, especially in retaining geometric structures.

This paper is arranged as follows. In Section 2, we give two models for the wavelet based inpainting problems according to the presence or absence of noise. In Section 3, we derive the Euler-Lagrange equations for the models and analyze their relationships to other wavelets based image processing tasks. We also prove the existence of the solutions and construct an nontrivial example to illustrate the non-uniqueness of the solutions. Section 4 presents numerical algorithms and schemes for solving the Euler-Lagrange equations. Generic numerical examples in Section 5 further highlight the

remarkable inpainting qualities of both the models and their numerical schemes.

2. TV Minimization Models for Wavelets Based Image Inpainting. In this section, we propose two TV regularized wavelet based image inpainting models depending on whether or not noise needs to be suppressed in the image.

We start with a standard image model,

$$z(x) = u_0(x) + n(x), \tag{1}$$

where $u_0(x)$ is the original noise free image and $n(x)$ the Gaussian white noise. We assume that the size of the image is $n \times m$. Let us denote the standard orthogonal wavelet transform of $z(x)$ by,

$$z(\alpha, x) = \sum_{j,k} \alpha_{j,k}\psi_{j,k}(x), \qquad j \in \mathbf{Z},\ k \in \mathbf{Z}^2. \tag{2}$$

(For tensor-product based multiresolution analysis in 2-D, there should be three mother wavelets $\psi^{(1)}, \psi^{(2)}$, and $\psi^{(3)}$, but for convenience we shall instead only use a single symbol ψ. No confusion will arise below since both our models and algorithms will not specifically differentiate them.) In wavelet based image representations, the coefficients $\alpha = \{\alpha_{j,k}\}$ are the values being stored. Notice that here the low and high frequency (or scale) coefficients are not being distinguished, while standard digital representations usually need to separate them. One reason to do so is for simplicity. A different reason is that in the proposed models and methods, we allow the missing or damaged coefficients to be in both the low and high frequency ranges. The models can automatically handle them differently if they belong to different frequency ranges, even though low frequency coefficients have completely different properties than the high frequency ones.

We remark that in the following models and analysis, we have employed *orthogonal wavelets* for convenience. All the analytical results and computational schemes can be easily modified for biorthogonal wavelets for which it suffices to distinguish the *analysis* and *synthesis* wavelets.

Damages (scratches and scars) in the wavelet domain cause loss of wavelet coefficients of $z(x)$ on the index region I, i.e., $\{\alpha_{j,k}\}$'s with $(j,k) \in I$ represent those wavelet components missing or damaged. The task of inpainting is to restore the missing coefficients in a *proper* manner, so that the image will have as much information being restored as possible.

As mentioned before, the inpainting problem usually allows more than one solutions and many different ways to fill in the missing coefficients, which lead to different reconstructions in the pixel domain. One often has to use proper regularization to guide the filling of missing coefficients. In many applications, it is crucial to have geometrical features (from available image information) propagated into the pixel domains of inpainting. For this reason, it is important to control the regularity in the pixel domain, so that broken or incomplete edges can be completed faithfully, and noise removed effectively.

With all these factors in mind, we now propose two variational models for wavelets based image inpainting.

If the target image is noiseless or the noise n is small enough to be negligible, one just needs to fill in the damaged wavelet coefficients and preserve the other coefficients. We propose a simple TV minimization scheme to fill in the missing coefficients.

Model I (for noiseless images):

$$\min_{\beta_{j,k}:(j,k)\in I} F(u,z) = \int_{\mathbf{R}^2} |\nabla_x u(\beta,x)|dx = \mathrm{TV}(u(\beta,x)), \tag{3}$$

where $u(\beta,x)$ has the wavelet transform:

$$u(\beta,x) = \sum_{j,k} \beta_{j,k}\psi_{j,k}(x), \qquad \beta = (\beta_{j,k}), \quad j \in \mathbf{Z},\ k \in \mathbf{Z}^2,$$

and subject to the constraint:

$$\beta_{j,k} = \alpha_{j,k}, \quad (j,k) \notin I,$$

where I is the inpainting index region. We remark that the derivative ∇u is often denoted by the Radon measure symbol Du in the standard literature on functions with bounded variations (BV).

In many applications, such as signal transmission in wireless channels, noise is unavoidably introduced in addition to the loss of data packages. More precisely, in addition to the possibility that some coefficients $\beta_{j,k}, (j,k) \in I$ can be completely lost or damaged, the remaining others $(\beta_{j,k}, (j,k) \notin I)$ can also be polluted by noise, which cannot be ignored. In this situation, we propose a second model for wavelet inpainting.

Model II (for noisy images):

$$\min_{\beta_{j,k}} F(u,z) = \int_{\mathbf{R}^2} |\nabla_x u(\beta,x)|dx + \sum_{(j,k)} \lambda_{j,k}(\beta_{j,k} - \alpha_{j,k})^2, \tag{4}$$

and the parameter $\lambda_{(j,k)}$ is zero if $(j,k) \in I$, the missing index set; otherwise, it equals a positive constant λ to be properly selected (see further discussions in the next section).

In the objective functions in (3) and (4), we use the total variation (TV) norm because it can retain sharp edges while reducing the noise and other oscillations, such as Gibbs' phenomena, in the reconstruction [59]. Our approach can be easily extended to include other regularizers, such as ones containing curvature [13]

The models are related to our earlier studies of TV model for wavelet based image denoising and compression [22]. The key difference between the models is that in Model I, the arguments in the TV minimization are restricted to the inpainting regions I only, the dimension of unknowns is the number of coefficients in I, while in Model II, the parameter λ is taken to be zero in the inpainting regions in the wavelet domain, in contrast to the standard denoising and compression models, where λ is usually taken to be a constant. This difference essentially puts no constraint on the missing wavelet coefficients so that they can change freely, and therefore restore the missing information.

We remark that unlike most image processing models, Model I does not require any user-defined parameter. This provides significant advantages for Model I over the other TV based image processing models. Of course, the preassumption for Model I is that the given image observation, or equivalently the available collection of its wavelet coefficients, is noiseless.

3. Analysis of the Models. For convenience, we shall assume in this section that the image domain is the entire plane $\Omega = \mathbf{R}^2$, and the gradient symbol ∇u represents $\nabla_x u(\beta, x)$. As common in the variational literature, the image u is always assumed to be smooth so that all the subsequent formal derivations of the Euler-Lagrange equations in 3.4 can be valid in the classical sense (see, e.g. Rudin-Osher-Fatemi [59]). Generally, the gradients involved must be properly understood in the settings of subdifferentials or distributions. On the other hand, following the work of Chan-Osher-Shen [14], the total variation measure allows a self-contained digital formulation on a general discrete lattice or graph, and most of the analytical complications can be avoided from a practical point of view.

3.1. Why the Hybrid Models. From the wavelet representation point of view, one naturally asks the following question:

"Can both models be expressed explicitly by the wavelet representation?"

More specifically, as in the celebrated denoising works by Donoho, DeVore, and their collaborators [29, 30, 26, 11], is there an *equivalent* model (to Model II, say) that is fully based on the wavelet coefficients in the classical form of:

$$F^*(\beta) = \Phi(|\beta_{j,k}|'s) + \sum_{(j,k)} \lambda_{j,k}(\beta_{j,k} - \alpha_{j,k})^2,$$

where $(|\beta_{j,k}|'s)$ denotes the sizes of all wavelet coefficients, and Φ a suitable function of all these sizes. By *equivalence* to model II, we mean there exist two fixed positive constants C_1 and C_2, independent of β or u, so that

$$C_1 \mathrm{TV}(u(\beta, x)) \le \Phi(|\beta_{j,k}|'s) \le C_2 \mathrm{TV}(u(\beta, x)). \tag{5}$$

More rigorously, we assume that Φ does not depend upon the particular (orthonormal) wavelets basis employed but the two constants C_1 and C_2 may.

The answer is negative, which reveals the major difference between our models and the classical wavelets denoising schemes based on Besov regularity conditions [11, 51]. Recall that the Besov regularity norm is defined in 2-D by

$$\begin{aligned} \|u\|_{\dot{B}^{\alpha}_{q}(L^p(\mathbf{R}^2))} &= \left(\int_0^{\infty} (\omega_p(u,h)h^{-\alpha})^q \, dh/h \right)^{1/q} \\ &\sim \left(\sum_j 2^{jq(\alpha+1-2/p)} \|\beta_{j,}\|_{l^p}^q \right)^{1/q}. \end{aligned}$$

Here the dot symbol in $\dot{B}^{\alpha}_{q}(L^p(\mathbf{R}^2))$ indicates the homogeneity of the Besov norm in discussion, $\|\beta_{j,}\|_{l^p}$ the sequence l^p-norm at each resolution j, and ω the p-modulus of continuity:

$$\omega_p(f,h) = \sup_{|a| \le h} \|f(x+a) - f(x)\|_{L^p(\mathbf{R}^2)}.$$

In fact, one has the following negative result for images with bounded variations [51].

THEOREM 3.1. *The space of $BV(\mathbf{R}^2)$ cannot be characterized by size properties on wavelet coefficients.*

This is mainly because there exist "rotations" (or unitary transforms) in $L^2(\mathbf{R}^2)$ that "swing" some BV images out of the BV space, which could not occur if (5) were true.

Furthermore, the wavelet coefficients vector β of a BV image lies somewhere strictly between l^1 and weak l^1, but cannot be characterized by either, according to the remarkable results of Yves Meyer [51], and Albert Cohen et al. [24].

The fact that a generic image of BV is beyond simple wavelet description is mainly due to the geometric nature of the total variation semi-norm, or more generally, the total variation as a Radon measure [37]. The preceding discussion has already revealed that the first variation of the total variation measure leads to the most important second order Euclidean geometric feature - the curvature

$$\kappa = \kappa(\beta, x) = \nabla \cdot \left[\frac{\nabla u(\beta, x)}{|\nabla u(\beta, x)|} \right].$$

Even more profound on the geometric nature is the celebrated co-area formula of Fleming-Rishel [35] and De Giorgi [36]:

$$\int_{\mathbf{R}^2} |\nabla u| dx = \int_{-\infty}^{\infty} \text{length}(\text{u} \equiv \gamma) \text{d}\gamma, \tag{6}$$

where $u \equiv \gamma$ denotes the γ-level curve for any $\gamma \in \mathbf{R}^2$. Therefore, the total variation Radon measure $|\nabla u|$ amounts to summing up the lengths of *all* the level lines of a given image u. For simplicity, u has been assumed to be smooth so that its level lines are well defined. For more general images with bounded variation, the above coarea formula can be updated to

$$\int_{\mathbf{R}^2} |Du| = \int_{-\infty}^{\infty} \text{Per}(\text{u} > \gamma) \text{d}\gamma.$$

Here $|Du|$ denotes total variation as a Radon measure, and $\text{Per}(\text{u} > \gamma)$ the perimeter of the Caccioppli set [37]

$$\{x \in \mathbf{R}^2 \mid u(x) > \gamma\}.$$

Classical wavelets, as space-scale representation tools, are however not originally motivated by, nor designed to handle explicitly, geometric information. This could at least shed some light on why generic BV images are beyond explicit descriptions based upon only the sizes of their wavelet coefficients. Many researchers have noticed this drawback, and proposed different ways to incorporate geometries in the study. Nowadays, geometric harmonic analysis, e.g. curvelets [6], is a hot research topic.

On the other hand, in computer vision as well as human vision, geometric information in images, such as edges, smoothness, junctions, and corners, are significant visual cues for successful perception (see, e.g., David Marr's work [50]). The space of functions with bounded variations, among all the familiar functional spaces in classical real analysis, is perhaps the simplest one that *legalizes* the existence of jumps or edges. Other image models such as the celebrated Mumford-Shah's object-edge model [52], often substantially increase the complexity in both theory and computation, by explicitly singling out the edge geometric feature.

To conclude, with wavelet coefficients inevitably polluted by noise and partially missing, it seems natural to explicitly enforce the edge geometric information using the total variation Radon measure. Such hybrid models (e.g., Model I and Model II) can faithfully inpaint the missing wavelet coefficients while retaining the sharpness of missing edges. Our later numerical results shall further confirm our claim.

3.2. Existence Theorems of Model I and II. In this section, we prove the existence theorems for both models I and II. The non-uniqueness issue will be addressed in the next subsection.

We take an elementary approach for proving the existence of solutions to Model I, while a more general one based on the direct method for Model II. The image domain is assumed to be the entire plane $\mathbf{R}^2$.

We must emphasize that unlike for more familiar restoration problems such as denoising and deblurring, the data loss in inpainting problems and its resultant lack of norm control in the missing regions impose new challenges on existence proof. For example, on a bounded Lipschitz image domain Ω, the existence of Chan and Shen's TV inpainting model [15] was proven by Chan, Kang, and Shen [13] under the assumption that $u(x) \in [0,1]$ on Ω. The restriction to $[0,1]$ conveniently leads to the boundedness of any minimizing inpainting sequence (u_n). In the following proof, however, we make no such assumptions on the boundedness of either the image domain Ω or the range of image gray values. Instead, to avoid the unnecessary complication due to boundary wavelets, we shall assume $\Omega = \mathbf{R}^2$, and further benefit as well from the scaling-invariant Poincaré Inequality on the entire plane to control the boundedness of any minimizing inpainting sequence.

Following the preceding notations, let I denote the set of indices associated with all the missing wavelets coefficients and $d = \#I < \infty$, the number of lost coefficients. Define two orthogonally complementing subspaces of $L^2(\mathbf{R}^2)$ according to I:

$$V_I = \text{span}\{\psi_{j,k} \mid (j,k) \in I\},$$
$$U_I = \text{closure}(\text{span}\{\psi_{j,k} \mid (j,k) \notin I\}).$$

Let Q_I and P_I denote the orthogonal projections onto V_I and U_I separately. Then

$$Q_I + P_I = Id, \qquad \text{the identity operator in } L^2(\mathbf{R}^2),$$

and $z_I = P_I z$ is the available observation while $Q_I z$ is lost during transmission.

We now first turn to the existence of Model I. Any inpainting candidate u can be decomposed to

$$u = u_I + v_I, \quad \text{with } u_I = P_I u, \quad v_I = Q_I u.$$

For Model I, z is assumed to be noiseless and $u_I = P_I z$ is therefore fixed. The only freedom comes from the v_I or β_I component. Write:

$$v_I = v_I(\beta_I, x), \quad \beta_I = \{\beta_{j,k} \mid (j,k) \in I\},$$

to indicate the dependence of v_I on the missing wavelet coefficients β_I. Define

$$F(\beta_I) = F(u,z) = \text{TV}(u_I + v_I(\beta_I, x)).$$

Then $F(\beta_I)$ could be considered as a function on $\mathbf{R}^d$.

THEOREM 3.2. *Assume that the mother wavelet $\psi(x)$ belongs to $\text{BV}(\mathbf{R}^2)$ and is compactly supported, which are true for most familiar wavelets (e.g., Haar wavelets, or any C^1 family) [25]. Also assume that u_I belongs to $\text{BV}(\mathbf{R}^2)$. Then the objective function $F(\beta_I)$ satisfies*

(a) $F(\beta_I)$ is (Lipschitz-) continuous; and
(b) $F(\beta_I) \to +\infty$ as $\beta_I \to \infty$ in $\mathbf{R}^d$.
As a result, the minimizer to $F(\beta_I)$ must exist.

Proof. By the assumption on the mother wavelet, $\psi_{j,k}$ belongs to $\mathrm{BV}(\mathbf{R}^2)$ for any $(j,k) \in I$. Since TV is a semi-norm, one has for any β_I and β'_I in $\mathbf{R}^d$,

$$\begin{aligned} |F(\beta_I) - F(\beta'_I)| &= |\mathrm{TV}(u_I + v_I(\beta_I, x)) - \mathrm{TV}(u_I + v_I(\beta'_I, x))| \\ &\le \mathrm{TV}(v_I(\beta_I, x) - v_I(\beta'_I, x)) \\ &= \mathrm{TV}(v_I(\beta_I - \beta'_I, x)) \\ &\le \|\beta_I - \beta'_I\|_{l^1} \max_{(j,k)\in I} \mathrm{TV}(\psi_{j,k}). \end{aligned}$$

This proves (a) since all norms in $\mathbf{R}^d$ are equivalent. By further noticing that $v_I = Q_I u$ is compactly supported, by Poincaré's inequality [37, 44], one has

$$\left(\int_{\mathbf{R}^2} |v_I|^2 dx \right)^{\frac{1}{2}} \le C \int_{\mathbf{R}^2} |\nabla v_I| dx = C \times \mathrm{TV}(v_I),$$

where the positive constant C is universal and independent of v_I, or equivalently β_I. Thus under a general orthonormal wavelet basis,

$$\begin{aligned} F(\beta_I) &= \mathrm{TV}(u_I + v_I(\beta_I, x)) \\ &\ge \mathrm{TV}(v_I(\beta_I, x)) - \mathrm{TV}(u_I) \\ &\ge C^{-1} \|v_I\|_{L^2} - \mathrm{TV}(u_I) \\ &= C^{-1} \|\beta_I\|_{l^2} - \mathrm{TV}(u_I) \to +\infty, \quad \text{as } \beta_I \to \infty. \end{aligned}$$

This establishes (b) and completes the existence proof for Model I. □

The proof for the existence of Model II inpainting has to take a turn, due to the aforementioned fact that there exists no simple and explicit description for the TV norm in the wavelets domain. A natural way to proceed is to deal with the physical image u directly, instead of its wavelet coefficients β.

Model II is to minimize the energy

$$F(u, z) = \int_{\mathbf{R}^2} |\nabla u| dx + \lambda \int_{\mathbf{R}^2} (u_I - z_I)^2 dx, \tag{7}$$

where $u_I = P_I u$ and $z_I = P_I z$. Unlike most other variational models in image processing, the incompleteness of data imposes a subtle challenge for proving the existence, because the lack of data (in the fitting term) results in an incomplete control over the global norms, which is however often crucial for establishing weak compactness of minimizing sequences in the direct method. For this purpose, Poincaré's inequality on the *entire* plane plays a fundamental role in the following proof.

THEOREM 3.3. *Suppose that the available set of wavelet coefficients α_{I^c} is in l^2, or equivalently,*

$$z_I = P_I z \in L^2(\mathbf{R}^2).$$

Then the minimizer to $F(u, z)$ in Model II (7) exists.

Proof. First, from the assumption it follows that for any admissible inpainting u, its u_I component must belong to $L^2(\mathbf{R}^2)$ due to the fitting term in $F(u, z)$. Since

$$u = Q_I u + P_I u = Q_I u + u_I,$$

and $Q_I u \in V_I \subset L^2(\mathbf{R}^2)$, it follows that an $F(u,z)$-admissible inpainting u must belong to $L^2(\mathbf{R}^2)$.

Since $u = 0$ is apparently admissible, there must exist a minimizing sequence $(u^i)_{i=1}^{\infty}$ for $F(u,z)$. Then $u^i \in L^2(\mathbf{R}^2)$, and

$$\int_{\mathbf{R}^2} |\nabla u^i| dx \leq F(u^i, z) \to \inf_u F(u,z), \quad i \to \infty.$$

In particular, the total variations of u^i's are bounded. Recall Poincaré's inequality in $\mathbf{R}^2$ [37, 44],

$$\left(\int_{\mathbf{R}^2} |u|^2 dx \right)^{\frac{1}{2}} \leq C \int_{\mathbf{R}^2} |\nabla u| dx,$$

for any $u \in L^2(\mathbf{R}^2)$ (whose total variation could be infinity), and a universal constant C independent of u. We thus conclude that (u^i) must be bounded in $L^2(\mathbf{R}^2)$.

As a result, on any *bounded* open domain $\Omega \subset \mathbf{R}^2$, the restriction of (u^i) must be bounded in $\mathrm{BV}(\Omega)$ (according to Schwarz's inequality). By the L^1 pre-compactness of bounded BV functions on finite domains and the diagonal selection procedure, one can find a subsequence of (u^i), still denoted by the same notation for convenience, such that

$$u^i \to u^*, \quad \text{as } i \to \infty \text{ in } L^1_{\mathrm{loc}}(\mathbf{R}^2),$$

for some locally integrable image u^*. In particular,

$$u^i \to u^*, \quad \text{weakly or in the distributional sense on } \mathbf{R}^2.$$

Then by the lower semi-continuity of the total variation semi-norm under L^1_{loc} topology [37], one has

$$\int_{\mathbf{R}^2} |\nabla u^*| dx \leq \liminf_{i \to \infty} \int_{\mathbf{R}^2} |\nabla u^i| dx.$$

By the lower semi-continuity of the L^2-norm under the weak topology, one has

$$\int_{\mathbf{R}^2} |u^*|^2 dx \leq \liminf_{i \to \infty} \int_{\mathbf{R}^2} |u^i|^2 dx.$$

Finally, since the mother wavelet is assumed to be compactly supported, it is easy to verify that the projection operator P_I maps compactly supported images to still compactly supported ones. As a result, the weak convergence of (u^i) implies

$$u^i_I = P_I u^i \to u^*_I = P_I u^*, \quad \text{weakly on } \mathbf{R}^2.$$

Then the lower semi-continuity of the L^2-norm yields

$$\int_{\mathbf{R}^2} |u^*_I - z_I|^2 dx \leq \liminf_{i \to \infty} \int_{\mathbf{R}^2} |u^i_I - z_I|^2 dx.$$

In combination, one concludes that $u^* \in L^2(\mathbf{R}^2)$ is admissible and

$$F(u^*, z) \leq \liminf_{i \to \infty} F(u^i, z) = \inf_u F(u, z).$$

Therefore u^* must be a minimizer, and

$$\beta^*_{j,k} = \langle u^*, \psi_{j,k} \rangle, \quad (j,k) \in I,$$

constitute an optimal set of inpainted wavelet coefficients under Model II, which completes the proof. □

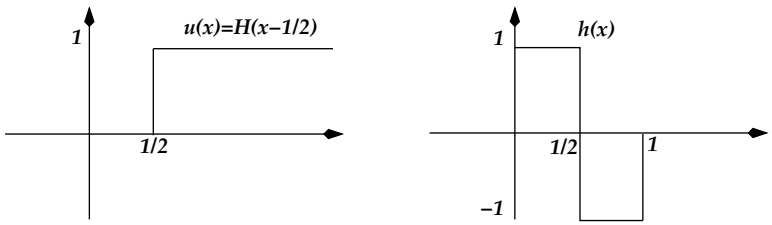

FIG. 1. *A 1-D ideal step-edge image u, and Haar's mother wavelet $h(x)$.*

3.3. Non-Uniqueness: An Example via Haar Wavelets. In this section, we show by a concrete 1-D example that the uniqueness of the proposed inpainting models is generally unguaranteed.

Unlike most other image restoration problems (e.g., denoising or deblurring), the solutions to inpainting models are often non-unique. For classical inpainting problems on pixel domains, this has been addressed by Masnou and Morel [49], and Chan and Shen [15]. In particular, the latter discussed the non-uniqueness issue also from the viewpoints of global pattern recognition as well as the ambiguity in human visual inference.

To proceed with our construction, first we define a noiseless 1-D signal or image u with an ideal step edge at $x = 1/2$:

$$u(x) = 1_{x \geq 1/2}(x) = H(x - 1/2),$$

where H denotes the canonical 0-1 Heaviside function. Let $\psi = h(x)$ be the mother Haar wavelet:

$$h(x) = 1_{[0,1/2)}(x) - 1_{[1/2,1)}(x),$$

normalized so that the L^2 norm is 1. Then all other basis wavelets are generated by

$$h_{j,k}(x) = 2^{j/2} h(2^j x - k), \quad j, k \in \mathbf{Z}.$$

Let $\beta_{j,k}$'s denote the wavelet coefficients of the ideal step edge u:

$$\beta_{j,k} = \langle u(x),\ h_{j,k}(x) \rangle = \int_{\mathbf{R}} u(x) h_{j,k}(x) dx.$$

Suppose that a receiver is able to receive all the wavelet coefficients of u, except for the single one

$$\beta_{0,0} = \langle u(x),\ h(x) \rangle = \int_{1/2}^{1} (-1) dx = -\frac{1}{2},$$

which is missing and unknown to the receiver. In this case, the inpainting index set is a singleton $I = \{(0, 0)\}$. Define

$$u_I = \sum_{(j,k) \notin I} \beta_{j,k} h_{j,k}(x),$$

which is the reconstruction of u assuming there is no $h_{0,0} = h(x)$ component. Then,

$$u_I(x) = u(x) - \beta_{0,0} h_{0,0}(x) = H(x - \frac{1}{2}) + \frac{1}{2} h(x) = \frac{1}{2}\ 1_{[0,1)}(x) + 1_{[1,\infty)}(x).$$

For each candidate $\beta_{0,0} = a \in \mathbf{R}$, define the reconstruction

$$u(a,x) = u_I(x) + ah(x) \tag{8}$$

$$= (\frac{1}{2} + a)1_{[0,1/2)}(x) + (\frac{1}{2} - a)1_{[1/2,1)}(x) + 1_{[1,\infty)}(x), \tag{9}$$

as in our Model I (since this is a noiseless example). Then Model I is to minimize the following single variable energy:

$$\min_a \int_{\mathbf{R}} |\nabla u(a,x)|dx = \min_a \mathrm{TV}(u(a,x)).$$

Here $|\nabla u|$ is understood in the Radon measure sense since $u(a,x)$ is discontinuous.

Recall in classical real analysis, that the total variation of a piecewise constant function $f(x)$ is precisely the sum of all absolute jumps:

$$\mathrm{TV}(f) = \sum_{x_i \in J} |f(x_i+) - f(x_i-)|,$$

where J denotes the collection of all jumps of f. Since $u(a,x)$ is indeed piecewise constant, we have according to (8), for any $a \in \mathbf{R}$,

$$\mathrm{TV}(u(a,x)) = |1/2 + a| + |2a| + |1/2 + a| = |1 + 2a| + |2a|.$$

As a result, the lower bound of the total variation energy is

$$\mathrm{TV}(u(a,x)) \geq |(1 + 2a) - 2a| = 1,$$

which can be achieved if and only if

$$-1 \leq 2a \leq 0, \qquad \text{or,} \qquad -\frac{1}{2} \leq a \leq 0.$$

In other words, taking any value of $a \in [-\frac{1}{2}, 0]$ minimizes the objective function in Model I, and therefore is a solution of the wavelet inpainting problem. This clearly shows that in this noiseless example, Model I could lead to multiple inpainting results.

We must emphasize, however, as well explained by Chan and Shen in [15], that non-uniqueness is not a drawback of any inpainting model. Rather, it is an intrinsic nature of the inpainting problem itself and differentiates image inpainting from other familiar image restoration tasks such as image denoising and deblurring.

3.4. Euler-Lagrange Equations. Let

$$\beta_I = \{\beta_{j,k} \mid (j,k) \in I\}$$

denote all the missing wavelet coefficients to be inpainted. Since it has been assumed that $\#I = d$, β_I can be considered as a vector in $\mathbf{R}^d$.

For Model I, one attempts to minimize

$$F(\beta_I) = F(u,z) = \int_{\mathbf{R}^2} |\nabla u(\beta,x)|dx.$$

For any missing index $(j,k) \in I$,

$$\begin{aligned} \frac{\partial F(\beta_I)}{\partial \beta_{j,k}} &= \int_{\mathbf{R}^2} \frac{\nabla u}{|\nabla u|} \cdot \frac{\partial \nabla u(\beta, x)}{\partial \beta_{j,k}} dx \\ &= \int_{\mathbf{R}^2} \frac{\nabla u}{|\nabla u|} \nabla \frac{\partial u(\beta, x)}{\partial \beta_{j,k}} dx \\ &= \int_{\mathbf{R}^2} \frac{\nabla u}{|\nabla u|} \cdot \nabla \psi_{j,k} dx. \end{aligned} \tag{10}$$

Equivalently, if one assumes that the mother wavelet ψ is compactly supported (as for Daubechies family of wavelets [25]) and at least Lipschitz continuous, integration-by-parts yields

$$\frac{\partial F(\beta_I)}{\partial \beta_{j,k}} = -\int_{\mathbf{R}^2} \nabla \cdot \left[\frac{\nabla u}{|\nabla u|} \right] \psi_{j,k} dx = -\langle \kappa, \psi_{j,k} \rangle, \tag{11}$$

where $\kappa = \nabla \cdot [\nabla u / |\nabla u|]$ is the celebrated curvature formula for the level lines of u. Thus this last formula clearly combines geometric information with wavelets decomposition. It is worth to note that this formula remains valid even for non-orthonormal wavelet basis.

Formula (10) on the other hand bears the advantage that it is well defined in the classical sense as long as both the mother wavelet ψ and the image u are Lipschitz continuous. That is, unlike formula (11), the image u needs not to be $C^{1,1}$. Furthermore, the differential $\nabla \psi_{j,k}$ also possesses the similarity relation:

$$\nabla \psi_{j,k}(x) = 2^j (\nabla \psi)_{j,k}, \quad x \in \mathbf{R}^2, \ k \in \mathbf{Z}^2.$$

Accordingly, it suffices to compute $\nabla \psi$ only once for the mother wavelet, and the rest can be obtained algebraically by dilation and translation.

It is also now a standard regularization technique to replace $|\nabla u|$ in the denominators of (10) and (11) by:

$$|\nabla u|_\epsilon = \sqrt{|\nabla u|^2 + \epsilon}, \qquad \text{with} \quad 0 < \epsilon \ll 1.$$

The small positive regularizer ϵ prevents the denominators from vanishing in numerical implementations. In fact, define the minimum-surface type of energy:

$$F_\epsilon(\beta_I) = \int_{\mathbf{R}^2} |\nabla u(\beta, x)|_\epsilon dx.$$

Then

$$\frac{\partial F_\epsilon(\beta_I)}{\partial \beta_{j,k}} = \int_{\mathbf{R}^2} \frac{\nabla u}{|\nabla u|_\epsilon} \cdot \nabla \psi_{j,k} dx = -\int_{\mathbf{R}^2} \nabla \cdot \left[\frac{\nabla u}{|\nabla u|_\epsilon} \right] \psi_{j,k} dx,$$

which are precisely the ϵ-regularized versions of (10) and (11). Our later computational schemes will be based on such regularization.

Similarly, for Model II with homogeneous Gaussian white noise, one can repeat the above computation and obtain, for any (j,k),

$$\begin{aligned} \frac{\partial F(\beta_I)}{\partial \beta_{j,k}} &= \int_{\mathbf{R}^2} \frac{\nabla u}{|\nabla u|} \cdot \nabla \psi_{j,k} dx + 2\lambda_{j,k}(\beta_{j,k} - \alpha_{j,k}) \\ &= -\int_{\mathbf{R}^2} \nabla \cdot \left[\frac{\nabla u}{|\nabla u|} \right] \psi_{j,k} dx + 2\lambda_{j,k}(\beta_{j,k} - \alpha_{j,k}). \end{aligned}$$

Here $\lambda_{j,k}$ is the binary function over indices:

$$\lambda_{j,k} = 0, \quad (j,k) \in I; \quad \lambda, \qquad \text{otherwise.} \tag{12}$$

Treating λ as a function on indices introduces more adaptivity or flexibility into most inpainting models [15] [13] [34]. For instance, if the noise is not spatially homogeneous so that the noise variance σ^2 on the wavelet coefficients are component-dependent:

$$\sigma^2 = \sigma_{j,k}^2, \quad \forall (j,k),$$

then instead of the binary choice in (12), one could allow λ to be a general function of indices with:

$$\lambda_{j,k} = 0, \quad (j,k) \in I; \quad \propto \frac{1}{\sigma_{j,k}^2}, \qquad \text{otherwise.}$$

In particular, if $\sigma_{j,k} = 0$ and the coefficients are noiseless, it reproduces Model I: for $(j,k) \in I$, $\lambda_{j,k} = 0$, and

$$-\int_{\mathbf{R}^2} \nabla \cdot \left[\frac{\nabla u}{|\nabla u|} \right] \psi_{j,k} dx = 0; \tag{13}$$

otherwise (corresponding to all the available noiseless coefficients), $\lambda_{j,k} = \infty$ and $\beta_{j,k} = \alpha_{j,k}$. Equation (13) is usually called the Euler-Lagrange equation for Model I.

Similarly, one can obtain the Euler-Lagrange equation for Model II as

$$-\int_{\mathbf{R}^2} \nabla \left(\frac{\nabla u}{|\nabla u|} \right) \psi_{j,k}(x) dx + 2\lambda_{j,k}(\beta_{j,k} - \alpha_{j,k}) = 0. \tag{14}$$

In the next section, we shall detail on the numerical computation of these two models.

4. Algorithm. There are many methods available in the literature to find the minimizers of the proposed models (e.g., properly modifying the lagged-diffusivity fixed point iterative schemes [1, 28]). The computation in the current work has been mainly based on the gradient descent approach, which by no means is the most efficient. The primary goal of the present work is however to explore the inpainting feasibility and qualities of the models rather than their numerics.

More precisely, as shown in the previous section, the minimizers of the proposed models satisfy the nonlinear Euler-Lagrange equations (13) and (14). We emphasize that in (13), there are only d equations, where d is the number of coefficients in the inpainting regions I, which can be much smaller than the total number of pixels, leading to more efficient solution procedures.

To find the minimizers, one just needs to solve for the solutions of the above Euler-Lagrange equations. Numerical methods for the TV models in pixel domain can be adapted to these equations. For instance, one can solve them by the method of gradient flow [59], which is achieved by introducing an artificial time variable and solving the following equations to steady states for Model I and Model II respectively,

$$(\beta_{j,k})_t = \int \nabla \left(\frac{\nabla u}{|\nabla u|} \right) \psi_{j,k}(x) dx, \quad (j,k) \in I, \tag{15}$$

and

$$(\beta_{j,k})_t = \int \nabla \left(\frac{\nabla u}{|\nabla u|} \right) \psi_{j,k}(x) dx - 2\lambda_{j,k}(\beta_{j,k} - \alpha_{j,k}). \tag{16}$$

The steady states refer to $(\beta_{j,k})_t = 0$. In this case, gradient flows (15) and (16) are reduced to the Euler-Lagrange equations (13) and (14).

Many numerical schemes can solve the above equations. For instance, we now describe a simple explicit finite difference algorithm that we employ to find the minimizers in this paper. To simplify the formulation, we introduce the standard finite difference notations, such as the forward differences $D_1^+ u_{k,l} = u_{k+1,l} - u_{k,l}$, $D_2^+ u_{k,l} = u_{k,l+1} - u_{k,l}$, and the backward differences $D_1^- u_{k,l} = u_{k,l} - u_{k-1,l}$, $D_2^- u_{k,l} = u_{k,l} - u_{k,l-1}$. The time step size is denoted by Δ_t and space grid size is $\Delta_x = \frac{1}{n}$. We also define $I_{j,k}$ as the characteristic function of inpainting regions I, i.e.

$$\chi_{j,k} = \begin{cases} 1 & (j,k) \in I \\ 0 & (j,k) \notin I \end{cases}$$

We note that it is important to evaluate the nonlinear term, which we denote as,

$$\text{WCURV} \equiv \int \nabla \left(\frac{\nabla u}{|\nabla u|} \right) \psi_{j,k}(x) dx$$

in both equations (15) and (16). This term is the curvature projected on the wavelet basis. However, the curvature is defined in the pixel domain. In this paper, we calculate it straightforwardly by transforming the coefficients to the pixel domain to compute the curvature, and then transform back to the coefficient domain. In detail, we calculate

$$u = \text{IWT}(\beta), \tag{17}$$

where IWT is the inverse wavelet transform. For all (i,j), compute

$$\begin{aligned} \text{curv}_{i,j} = D_1^- \left(\frac{D_1^+ u_{i,j}}{\sqrt{|D_1^+ u_{i,j}|^2 + |D_2^+ u_{i,j}|^2 + \epsilon}} \right) \\ + D_2^- \left(\frac{D_2^+ u_{i,j}}{\sqrt{|D_1^+ u_{i,j}|^2 + |D_2^+ u_{i,j}|^2 + \epsilon}} \right), \end{aligned} \tag{18}$$

where ϵ is a small positive number which is used to prevent the numerical blow-up when $\sqrt{|D_1^+ u_{i,j}|^2 + |D_2^+ u_{i,j}|^2} = 0$. In fact, this modification is the standard regularization technique described in Section 3.4. Then one computes the curvature projection on the wavelet basis by

$$\text{WCURV} = \text{FWT}(\text{curv}), \tag{19}$$

where FWT is forward wavelet transform.

The complete algorithm can be summarized by the following pseudo-code.

Algorithm:

(1) Start with $n = 0$ and initial guess $\beta_{j,k}^{new} = \alpha_{j,k}\chi_{j,k}$. Set $\beta_{j,k}^{old} = 0$, and the initial error $E = \|\beta^{new} - \beta^{old}\|_2$.
(2) While $i \leq N$ or $E \leq \delta$, do
- Set $\beta^{old} = \beta^{new}$.
- Calculate WCURV by (17), (18) and (19).
- For all (j,k), update

$$\beta_{j,k}^{new} = \beta_{j,k}^{old} + \frac{\Delta_t}{\Delta_x}\gamma_{j,k},$$

where $\gamma_{j,k}$ is defined by

$$\gamma_{j,k} = \beta_{j,k}^{TV}\chi_{j,k}$$

for Model I, and by

$$\gamma_{j,k} = \beta_{j,k}^{TV} - 2\lambda(\beta_{j,k} - \alpha_{j,k})(1 - \chi_{j,k})$$

for Model II respectively.
- Compute error $E = \|\beta^{new} - \beta^{old}\|_2$, and set $i = i + 1$.
- End the while loop.

5. Examples. To test the models, the standard Peak Signal to Noise Ratio (PSNR) is employed to quantify the performance of inpainting:

$$\text{PSNR} = 10\log_{10}(\frac{255^2}{\|u - u_0\|_2^2})(dB),$$

where 255 is the maximum intensity value of gray scale images, u_0 the noise free original image, and $\|\cdot\|_2$ the standard L^2 norm. As usual, larger PSNR values signifies better performance. In addition, we shall also highlight the performance of restoring sharp edges and other geometric features, which cannot be reflected through PSNR measurement. In all examples shown here, we use Daubechies 7-9 biorthogonal wavelets with symmetric extensions at the boundaries.

In the first example, we apply our two models to a synthetic image shown on the left panel of Figure 2. The image contains different geometrical features with different intensity values. The picture in the middle is obtained by losing (setting to zero) 50% of its wavelet coefficients randomly, resulting in PSNR $= 9.5(dB)$. Observe that there are no well defined inpainting regions in the pixel domain. The black dots in the rightmost panel show the indices of lost wavelet components. The frequency indices have been arranged in the standard manner with upper left corner storing the low-low frequencies, and lower right portion the high-high ones. The random and uncontrollable loss of low-resolution components results in the chunky "stains" in the middle image, while the high ones smear the original sharp edges. Moreover, different regions have different severity of damage which are certainly inhomogeneous in the image domain.

The inpainted images using our Model I and II are plotted in Figure 3 (with $\lambda = 10$ for Model II). Both models can fill in the missing homogeneous information properly, as well as restore the sharp edges and geometrical shapes. The PSNR are $29.4(dB)$ and $26.4(dB)$ for the left and middle respectively. Notice how surprisingly well the models have performed.

The right panel of Figure 3 shows the performance improvement measured by PSNR v.s. the severity of the damage. The horizontal axis represents the percentage

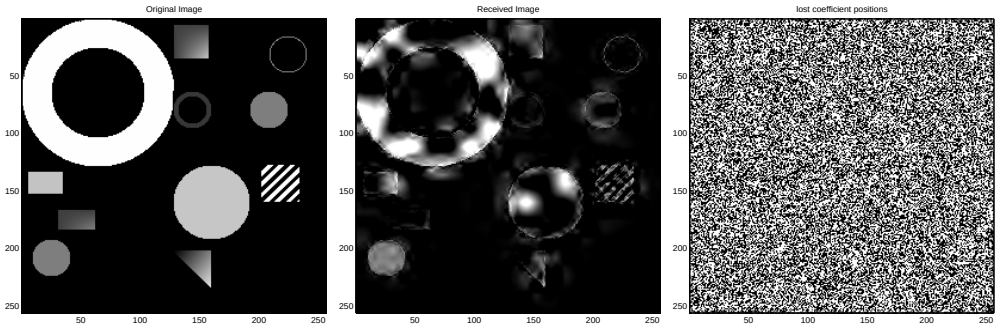

FIG. 2. *Left: Original synthetic image. Middle:* 50% *of the wavelet coefficients are randomly lost, including some low frequency coefficients, which results in large damaged regions in the pixel domain. Notice that there are no well defined inpainting regions in the pixel domain.* PSNR $= 9.5(dB)$. *Right: The index picture shows the locations (black) of missing wavelet coefficients. The upper left corner stores the low-low frequencies and the lower right portion the high-high ones.*

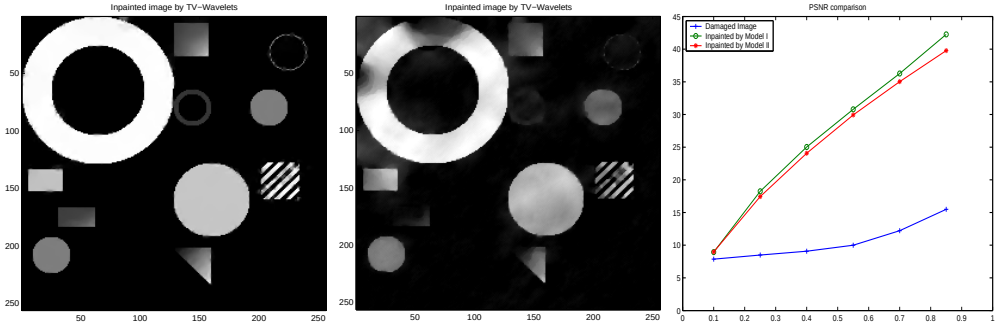

FIG. 3. *Restored images by Model I (left,* PSNR $= 29.4(dB)$*) and Model II (middle,* PSNR $= 26.5(dB)$*). They not only fill in missing regions properly, but also restore the sharp edges and geometrical shapes. The rightmost panel shows the performance comparisons of Model I and Model II with different level of damages. For the horizontal axis, for example,* $p = 0.85$ *means that* $1 - p = 15\%$ *of wavelet components are lost. The numerical curves in the rightmost panel show that both models can dramatically improve image qualities.*

of retained wavelet coefficients, so that the smallest left end corresponds to the most severe loss. The y-axis is the performance measure PSNR. The curve with circles is for Model I while that marked by stars is for Model II. They are plotted against the original damaged image (marked by crosses). Notice the dramatic improvement in PSNR (more than $10(dB)$) even when more than 70% wavelet coefficients are lost. The plot clearly shows the expected trend that larger improvement can be achieved for less loss. In addition, it also indicates that for noise free images, Model I outperforms Model II though both have performed surprisingly well.

In addition to the clear improvement measured by PSNR shown in Figure 3, both models improve the visual quality dramatically well. For better comparison, we further show the performance of Model I and II on two images with different levels of damage in Figure 4 and 5. Figure 4 shows 15% random loss, corresponding to the rightmost end of the curve panel in Figure 3. Figure 5 depicts the performance on a damaged image with severe wavelets loss of 90%, corresponding to the leftmost end of the curve panel.

Next, Figure 6 shows the performance on a noisy image (with PSNR $= 9.2(dB)$).

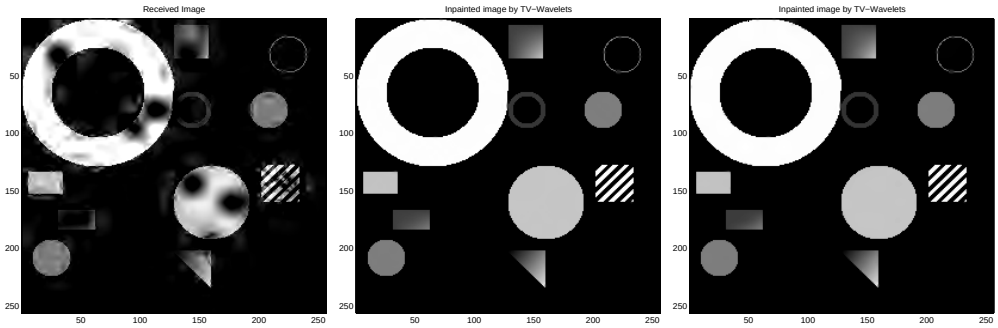

FIG. 4. *Left: Damaged image with* 15% *wavelet coefficients randomly lost. Restored images by Model I (middle,* PSNR = 42.3(dB)*) and Model II (right,* PSNR = 39.8(dB)*). Both inpainted images well agree with the original noise free image.*

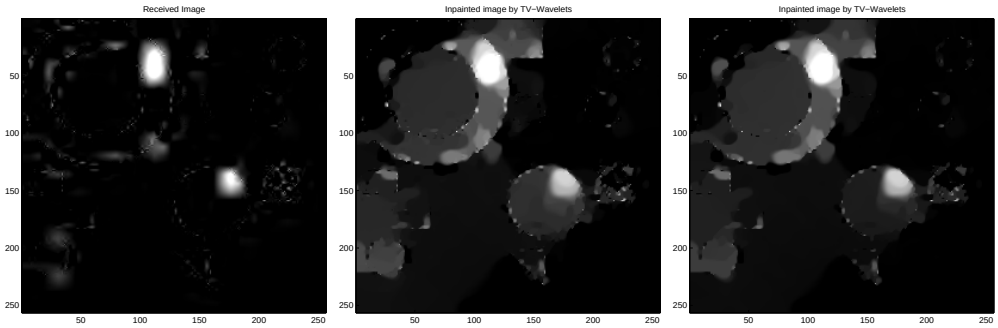

FIG. 5. *Left: Damaged image with* 90% *wavelet coefficients randomly lost. Restored images by TV wavelet image inpainting Model I (middle,* PSNR = 8.9(dB)*) and Model II (right,* PSNR = 9.0(dB)*). Both inpainted images can only restore partial geometry information since too many coefficients have been lost.*

The results clearly show that Model I can recover the geometrical features of the image, but can not suppress the noise in the reconstruction. The PSNR is improved to 15.1(dB). While Model II with parameter $\lambda = 10$ can perform both tasks of inpainting and denoising at the same time. The PSNR is 19.6(dB), which certainly outperforms Model I in the noise case. To complete the comparison, we plot the similar curves for PSNR improvements v.s. the percentage of retained coefficients for the noisy case and show them in Figure 7. As one can see, Model II outperforms Model I in the noise case, and Model I can not reduce the damage caused by the noise.

The next example in Figure 8 further investigates an intriguing extreme situation when all but one coefficients in the low-low subband are lost. Unlike conventional wavelets approximation, the other high bands are still retained. The resulting picture is shown on the right panel of Figure 8. The inpainted picture (by Model I) is shown on the left panel of Figure 9. Model I almost perfectly recovers the square with PSNR = 61.0(dB). The right panel of Figure 9 shows a typical slice of the recovered square, which is almost indistinguishable from the original. It shows that the proposed TV based inpainting model can recover the low frequency coefficients as well as the high ones.

What happens if all the low-low wavelet components are lost? The example in

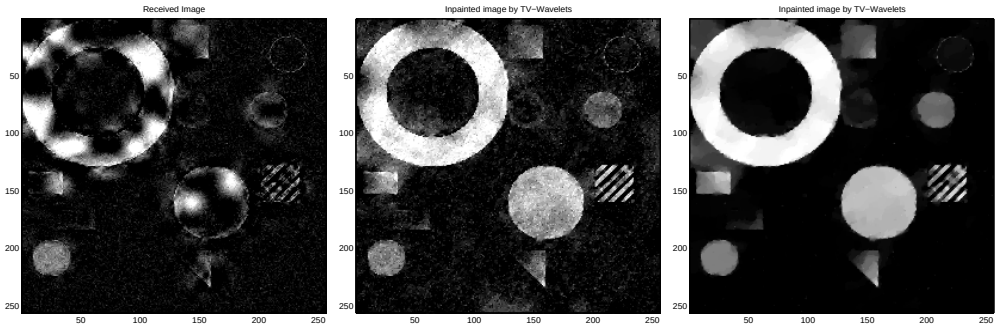

FIG. 6. *Left: A noisy image with* 50% *wavelet coefficients randomly lost. Middle: inpainted image by Model I. The geometrical features are restored, but the noise is not removed,* PSNR $=$ $15.1(dB)$. *Right: inpainted image by Model II with* $\lambda = 10$. *Notice how well the damaged geometrical features are restored and noise removed.* PSNR $= 19.6(dB)$.

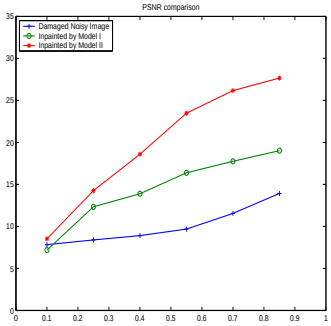

FIG. 7. *The performance comparisons of Model I and Model II with different level of damages for noisy images. It shows that both models can substantially improve image qualities while Model II can more effectively remove noises.*

Figure 10 answers the question. The inpainted image in the middle looks like the original square but the intensity values are wrong, as seen in the slice plotting in the right panel. The solid line is the original square, and the dotted for the damage image, which oscillates and loses all intensities in the middle of the square. The dash-dotted line is the output from Model I whose values are very different from the original ones. However, the inpainted image well recovers the heights of the jumps due to the retained high-band information. However, if one retains any one nonzero low frequency coefficient as in the preceding example of Figure 9, the intensities can also be perfectly determined.

In the next set of examples, we apply the models to a real noisy picture (the left panel of Figure 11) downloaded from the Internet. Similar to the first example, 50% of the wavelet coefficients are randomly lost, including some low frequency coefficients (the right panel of Figure 11). The PSNR is $10.9(dB)$. Again, there are no well defined inpainting regions in this example. We show the restored images by using Model I (left) and II (right) in Figure 12. They fill in the black regions properly, and retain the sharp edges. Moreover, one can also observe that some detail information (such as the texture of the tie) is recovered surprisingly well. This is due to the retained high frequency wavelet coefficients which contain the fine structure. Their respective PSNR's are $18.8(dB)$ and $18.7(dB)$.

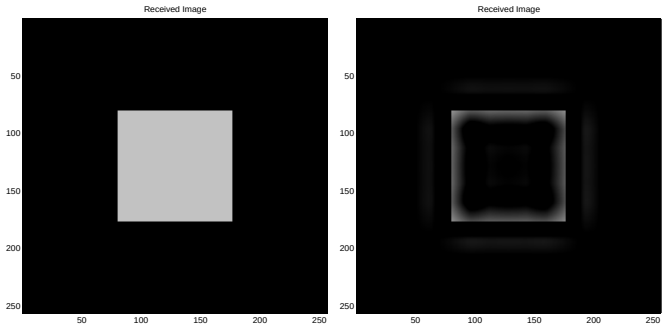

FIG. 8. *Left: An ideal image. Right: Damaged image with only one available non-zero coefficient in the low-low subband (but no loss in all other high resolution subbands).* PSNR $= 11.2(dB)$.

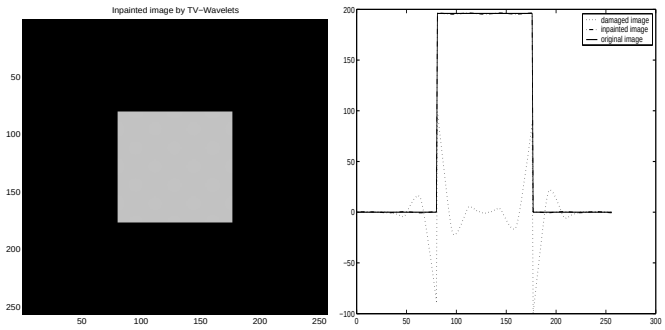

FIG. 9. *Left: The inpainted image by Model I. It almost perfectly recovers the square.* PSNR $=$ $61.0(dB)$. *Right: A horizontal slice of the inpainted image, which shows that the reconstruction coincides well with the original one.*

To further confirm the inpainting capability of the proposed models, we specially investigate the case where large regions in the low-low subband are lost. We show the picture on the left panel of Figure 13 with PSNR $= 13.1(dB)$. In this case, the standard inpainting methods cannot fill in the large missing region properly, while the proposed models can recover the image and improve the quality drastically. This is mainly because there is still some information available from the retained wavelet coefficients on the dark regions in the pixel domain. As seen on the right panel of Figure 13, we demonstrate the image obtained by using Model I. PSNR of the inpainted image is improved to $22.0(dB)$.

6. Conclusion. We have presented two models for restoring arbitrary number of coefficients with arbitrary locations of wavelet coefficients for images with or without noise. The idea is to use explicit regularization (i.e., the TV Radon measure and the BV image model) in the pixel domain to control and restore wavelet coefficients in the wavelet domain. Existence and uniqueness of the models have been rigorously investigated. We have shown through synthetic and real images that both models are very effective for restoring geometric features as well as filling in smooth regions, even with relatively large number of randomly lost coefficients uncontrollably spread across all resolutions.

REFERENCES

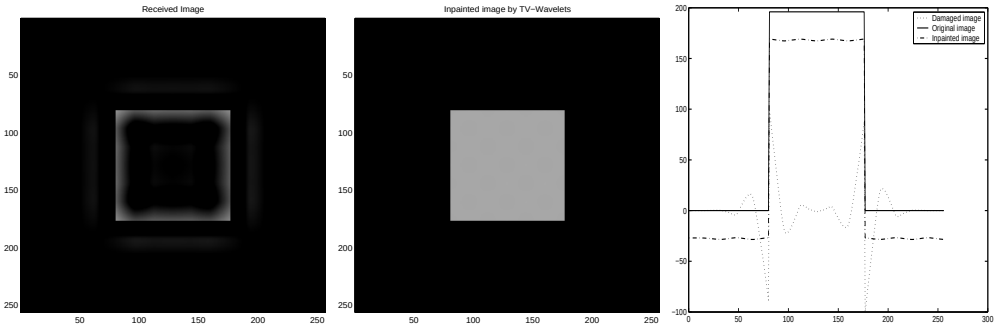

FIG. 10. *Left: The damaged image with all the low-low components missing (but no loss in all other high resolution subbands). Middle: The inpainted image by Model I, it looks like a perfect square is recovered, but their intensities are all wrong. Right: the cross plot of in the middle of the square of the inpainted image. The solid line is the original square, the dotted line is the damaged image and the dash-dotted line is the inpainted image. Clearly, the intensities are all wrong even thought the size of the jumps are perfectly reconstructed.*

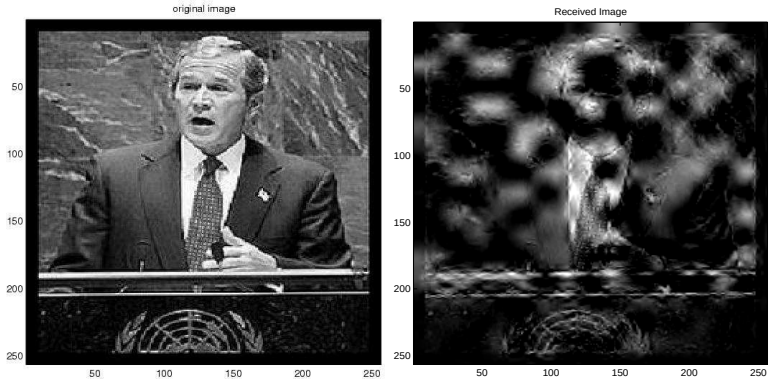

FIG. 11. *Left: Original noisy image. Middle:* 50% *of the wavelet coefficients are randomly lost, including some low frequency coefficients. Notice the severe damage in the pixel domain.* PSNR $= 10.9(dB)$.

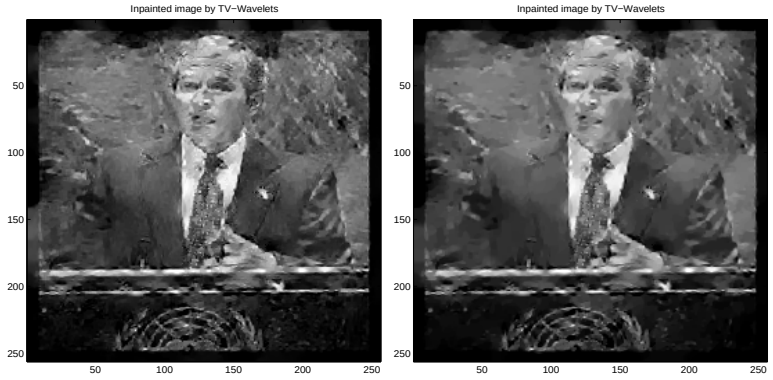

FIG. 12. *Restored images by Model I (left) and Model II (right). They both fill in the blank regions properly, and retain the sharp edges. One can even observe some detailed information such as the texture of the tie in the inpainted image. The corresponding* PSNR*'s are* $18.8(dB)$ *and* $18.7(dB)$ *separately.*

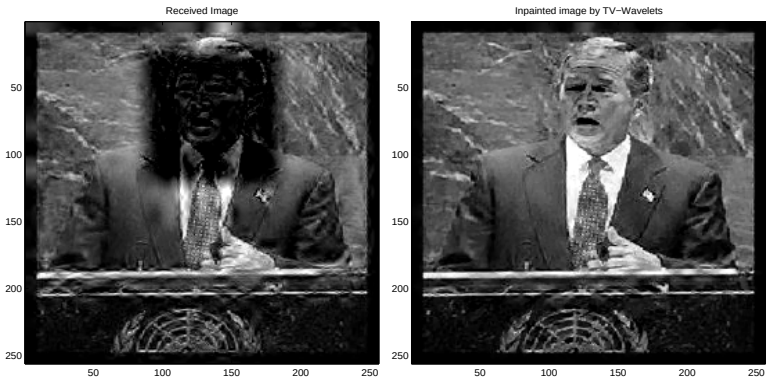

FIG. 13. *Left: Damaged image with a square region missing in the low-low subband, in addition to the randomly lost* 30% *high frequency coefficients.* PSNR $= 13.1(dB)$. *Right: Restored images by Model I.* PSNR $= 22.0(dB)$.

[1] R. Acar and C. R. Vogel. Analysis of total variation penalty methods for ill-posed problems. *Inverse Prob.*, 10:1217–1229, 1994.

[2] C. Ballester, M. Bertalmio, V. Caselles, G. Sapiro and J. Verdera, *Filling-in by Joint Interpolation of Vector Fields and Grey Levels*, IEEE Trans. Image Processing, 10(8), 2001, 1200-1211.

[3] M. Bertalmio, A.L. Bertozzi, and G. Sapiro. *Navier-Stokes, fluid dynamics, and image and video inpainting*, 2001 IEEE Conference on Computer Vision and Pattern Recognition. December. Kauai, Hawaii. Available at http://www.ece.umn.edu/users/marcelo/final-cvpr.pdf.

[4] M. Bertalmio, G. Sapiro, V. Caselles and C. Ballester, *Image Inpainting,* Tech. Report, ECE-University of Minnesota, 1999.

[5] M. Bertalmio, L. Vese, G. Sapiro and S. Osher, *Simultaneous Structure and Texture Image Inpainting*, UCLA CAM Report 02-47, July 2002,

[6] E. Candès and D. Donoho, *Curvelets - A Surprisingly Effective Nonadaptive Representation for Objects with Edges*, Curves and Surfaces, L. L. Schumaker et al. Eds, Vanderbilt University Press, Nashville, TN. 1999.

[7] E. J. Candès, and F. Guo. *Edge-preserving Image Reconstruction from Noisy Radon Data*, (Invited *Special Issue of the Journal of Signal Processing on Image and Video Coding Beyond Standards.*), 2001.

[8] E. Candès, J. Romberg and T. Tao, *Robust Uncertainty Principles: Exact Signal Reconstruction from Highly Incomplete Frequency Information*, Preprint: arXiv:math.GM/0409186, Sept. 2004.

[9] E. Candès, and T. Tao, *Near Optimal Signal Recovery From Random Projections and Universal Encoding Strategies*, Preprint, submitted to IEEE Information Theory, Oct. 2004.

[10] V. Caselles, R. Kimmel and G. Sapiro, *On Geodesic Active Contours*, Int. Journal of Computer Vision, 22(1), 1997, 61-79.

[11] A. Chambolle, R. A. DeVore, N.-Y. Lee, and B. J. Lucier. *Nonlinear wavelet image processing: variational problems, compression and noise removal through wavelet shrinkage.* IEEE Trans. Image Processing, 7(3):319–335, 1998.

[12] A. Chambolle and P. L. Lions. Image recovery via Total Variational minimization and related problems. *Numer. Math.*, 76:167–188, 1997.

[13] T. F. Chan, S. H. Kang and J. Shen, *Euler's Elastica and Curvature Based inpainting*, SIAM J. Appl. Math., 63(2) (2002), 564-592.

[14] T. F. Chan, S. Osher, and J. Shen, *The Digital TV Filter and Nonlinear Denoising*, IEEE Trans. Image Process., 10(2), pp. 231-241, 2001.

[15] T. F. Chan and J. Shen, *Mathematical Models for Local Non-Texture Inpainting*, SIAM J. Appl. Math., 62(3) (2002), 1019-1043.

[16] T. F. Chan and J. Shen, *Morphologically Invariant PDE Inpaintings*, UCLA CAM Report 01-15, 2001.

[17] T. F. Chan, J. Shen, and L. Vese, *Variational PDE Models in Image Processing*, Notices of AMS, Vol 50, No. 1, January 2003.

[18] T. F. Chan and L. Vese, *Active Contour Without Edges* Submit to IEEE Tran. on Image Proc., 1998.
[19] T. F. Chan and C. K. Wong, *Total Variation Blind Deconvolution*, IEEE Trans. Image Processing, 7 (1998), pp. 370-375.
[20] T. F. Chan and H. M. Zhou, *ENO-wavelet Transforms for Piecewise Smooth Functions*, SIAM J. Numer. Anal., Vol 40, No. 4 (2002), 1369–1404;
[21] T. F. Chan and H. M. Zhou, *Total Variation Minimizing Wavelet Coefficients for Image Compression and Denoising*, submitted to SIAM Journal on Scientific Computing.
[22] T. F. Chan and H. M. Zhou, *Optimal Constructions of Wavelet Coefficients Using Total Variation Regularization in Image Compression*, CAM Report, No. 00-27, Dept. of Math., UCLA, July 2000.
[23] M. Y. Cheng, H. Y. Huang and A. W. Y. Su, *A NURBS-based Error Concealment Techniques for Corrupted Images from Packet Loss*, in Proc. ICIP, bf 2, 2002, pp705-708.
[24] A. Cohen, R. DeVore, P. Petrushev, and H. Xu. *Nonlinear approximation and the space $BV(R^2)$.* Amer. J. Math., 121:587–628, 1999.
[25] I. Daubechies. *Ten lectures on wavelets.* SIAM, Philadelphia, 1992.
[26] R. A. DeVore, B. Jawerth, and B. J. Lucier. *Image compression through wavelet transform coding.* IEEE Trans. Information Theory, 38(2):719–746, 1992.
[27] L. Demanet, B. Song and T. Chan, *Image Inpainting by Correspondence Maps: a Deterministic Approach*, UCLA CAM Report 03-40, August 2003.
[28] D. Dobson and C.R. Vogel, *Convergence of An Iterative Method for Total Variation Denoising*, SIAM Journal on Numerical Analysis, 34 (1997), pp. 1779-1971.
[29] D. L. Donoho. *De-noising by soft-thresholding.* IEEE Trans. Information Theory, 41(3):613–627, 1995.
[30] D. L. Donoho and I. M. Johnstone. *Ideal spacial adaption by wavelet shrinkage.* Biometrika, 81:425–455, 1994.
[31] D. Dugatkin, H. M. Zhou, T. F. Chan and M. Effros, *Lagrangian Optimization of A Group Testing for ENO Wavelets Algorithm*, Proceedings to the 2002 Conference on Information Sciences and Systems, Princeton University, New Jersey, March 20 - 22, 2002.
[32] S. Durand and J. Froment, *Artifact Free Signal Denoising with Wavelets*, in Proceedings of ICASSP'01, volume 6, 2001, pp. 3685-3688.
[33] M. Elad, J-L. Starck, P. Querre and D. Donoho, *Simultaneous Cartoon and Texture Image Inpainting Using Morphological Component Analysis (MCA)*, to appear in the J. on Applied and Computational Harmonic Analysis.
[34] S. Esedoglu and J. Shen. Digital inpainting based on the Mumford-Shah-Euler image model. *European J. Appl. Math.*, 13:353–370, 2002.
[35] W. H. Fleming and R. Rishel. *An integral formula for total gradient variation.* Arch. Math., 11:218–222, 1960.
[36] E. De Giorgi. *Complementi alla teoria della misura $(n-1)$-dimensionale in uno spazio n-dimensionale.* Sem. Mat. Scuola Norm. Sup. Pisa, 1960-61.
[37] E. Giusti. *Minimal Surfaces and Functions of Bounded Variation.* Birkhäuser, Boston, 1984.
[38] *Special Issue on Partial Differential Equations and Geometry-Driven Diffusion in Image Processing and Analysis*, IEEE Tran. on Image Proc., Vol. 7, No. 3, Mar. 1998.
[39] P. C. Hansen, *The L-curve and Its Use in the Numerical Treatment of Inverse Problems*, Tech. Report, IMM-REP 99-15, Dept. of Math. Model., Tech. Univ. of Denmark, 1999.
[40] S. S. Hemami and R. M. Gray, *Subband-coded Image Reconstruction for Lossy Packet Networks*, IEEE Trans. Image Proc., 6:4, Apr. 1997, pp 523-539.
[41] H. Igehy and L. Pereira, *Image Replacement Through Texture Synthesis*, Proceedings to IEEE ICIP, 1997.
[42] K.-H. Jung, J.-H. Chang, and C. W. Lee, *Error Concealment Technique Using Data for Block-Based Image Coding*, SPIE, 2308,(1994), 1466-1477.
[43] Sung Ha Kang, Tony F. Chan and Stefano Soatto, *Inpainting from Multiple View*, UCLA CAM Report 02-31, May 2002.
[44] E. H. Lieb and M. Loss. *Analysis.* Amer. Math. Soc., second edition, 2001.
[45] F. Malgouyres, *Increase in the Resolution of Digital Images: Variational Theory and Applications*, Ph.D. thesis, Ecole Normale Supérieure de Cachan, 2000, Cachan, France.
[46] F. Malgouyres, *Mathematical Analysis of a Model Which Combines Total Variation and Wavelet for Image Restoration*, Journal of information processes, 2:1, 2002, pp 1-10.
[47] F. Malgouyres and F. Guichard, *Edge Direction Preserving Image Zooming: a Mathematical and Numerical Analysis*, SIAM, J. Num. Anal., 39:1, 2001, pp 1-37.
[48] L. Moisan, *Extrapolation de Spectre et Variation Totale Ponderee*, actes du GRETSI, 2001.
[49] M. Masnou and J. Morel, *Level-lines Based Disocclusion*, IEEE ICIP, October, 1998, 259-263.

[50] D. Marr. *Vision*. Freeman, San Francisco, 1980.
[51] Y. Meyer. *Oscillating Patterns in Image Processing and Nonlinear Evolution Equations*, volume 22 of *University Lecture Series*. AMS, Providence, 2001.
[52] D. Mumford and J. Shah. *Optimal approximations by piecewise smooth functions and associated variational problems.* Comm. Pure Applied. Math., 42:577–685, 1989.
[53] M. Nitzberg, D. Mumford, and T. Shiota. *Filtering, Segmentation, and Depth*. Lecture Notes in Comp. Sci., Vol. 662. Springer-Verlag, Berlin, 1993.
[54] Yan Niu and T. Poston, *Harmonic postprocessing to conceal for transmission errors in DWT coded images*. preprint, Institute of Eng. Sci., National Univ. of Singapore, 2003.
[55] J. W. Park and S. U. Lee, *Recovery of Corrupted Image Data Based on the NURBS Interpolation*, IEEE Trans. Circuits Syst. Video Tech., 9:7, Oct. 1999, pp 1003-1008.
[56] I. Peterson, *Filling in Blanks*, Science News, Vol. 161/19, May 11, 2002.
[57] S. Rane, J. Remus, and G. Sapiro, *Wavelet-domain reconstruction of lost blocks in wireless image transmission and packet-switched networks*. IEEE ICIP, 2002.
[58] S. Rane, G. Sapiro and M. Bertalmio, *Structure and texture filling-in of missing image blocks in wireless transmission and compression applications.* IEEE Trans. Image Processing 12, pp 296-303, 2003
[59] L. Rudin, S. Osher and E. Fatemi, *Nonlinear Total Variation Based Noise Removal Algorithms*, Physica D, Vol 60(1992), pp. 259-268.
[60] G. Sapiro, *Geometric Partial Differential Equations and Image Processing*, Cambridge University Press, 2001.
[61] G. Sapiro and A. Tannenbaum, *Affine Invariant Scale-Space*, Internet. J. Comput. Vision, 11 (1993), pp. 25-44.
[62] J.L. Starck, M. Elad and D. Donoho. *Image Decomposition via the Combination of Sparse Representations and a Variational Approach*. to appear in the IEEE Trans. Image Processing.
[63] G. Strang and T. Nguyen. *Wavelets and Filter Banks*. Wellesley-Cambridge Press, Wellesley, MA, 1996.
[64] Y. Wang, and Q. F. Zhu, *Error Control and Concealment for Video Communication: A Review*, Proc. IEEE, vol 86, no. 5, pp. 974-997.
[65] A. Yezzi, A. Tsai and A. Willsky, *A Fully Global Approach to Image Segmentation via Coupled Curve Evolution Equations*, Submitted to Journal of Visual Communication and Image Representation.